ANL-6845 ANL-6845

Argonne National Laboratory

STUDIES OF FAST REACTOR FUEL ELEMENT BEHAVIOR UNDER TRANSIENT HEATING TO FAILURE

II. In-pile Experiments on UO_2 Samples in the Absence of Coolant

by

C. E. Dickerman, L. E. Robinson,
E. S. Sowa, and S. B. Skladzien

Printed in USA. Price $3.00. Available from the Clearinghouse for Federal Scientific and Technical Information, National Bureau of Standards, U. S. Department of Commerce, Springfield, Virginia

ANL-6845
Reactor Technology
(TID-4500, 39th Ed.)
AEC Research and
Development Report

ARGONNE NATIONAL LABORATORY
9700 South Cass Avenue
Argonne, Illinois 60440

STUDIES OF FAST REACTOR FUEL ELEMENT BEHAVIOR UNDER TRANSIENT HEATING TO FAILURE

II. IN-PILE EXPERIMENTS ON UO_2 SAMPLES IN THE ABSENCE OF COOLANT

by

C. E. Dickerman and L. E. Robinson
Reactor Physics Division

and

E. S. Sowa and S. B. Skladzien
Reactor Engineering Division

January 1965

Part I was ANL-6334

Operated by The University of Chicago
under
Contract W-31-109-eng-38
with the
U. S. Atomic Energy Commission

TABLE OF CONTENTS

LIST OF FIGURES

LIST OF FIGURES

LIST OF FIGURES

LIST OF TABLES

STUDIES OF FAST REACTOR FUEL ELEMENT BEHAVIOR UNDER TRANSIENT HEATING TO FAILURE

II. In-pile Experiments on UO_2 Samples in the Absence of Coolant

by

C. E. Dickerman, L. E. Robinson,
E. S. Sowa, and S. B. Skladzien

I. INTRODUCTION

There is an increasing interest in the use of fissile refractory compounds as fuels in fast power reactors because of their high-temperature capabilities and the promise of high burnup. At Argonne National Laboratory, research is being performed in a spectrum of these materials including the oxides, carbides, and sulfides of uranium, plutonium, and thorium. Although one or more of the other compounds may prove to be more desirable for specific applications than uranium dioxide, it is at present a better-known material than its potential competitors.

Because of its comparatively low thermal conductivity and tensile strength, and the presence of void content, even in fired UO_2 bodies, there is presented, in principle at least, a set of possible safety problems for UO_2 fast-reactor fuel elements that are different from those of one-piece metallic elements. First, because of the well-known cracking of uranium oxide pellets, concern has been generated that the oxide fuel element does not provide a reliable prompt axial thermal expansion (even under conditions of negligible restraint from cladding, etc). Second, under conditions of transient heating, unrestrained pellets may shift their axial position, thus providing an erratic axial expansion or contraction. Third, under transient heating, oxide cracking and/or plastic deformation may result in "slumping" or axial compaction of fuel, which would reduce any effective prompt expansion coefficient or possibly produce a sudden "step" axial contraction.(1)

Some question has also arisen whether an oxide fuel element, subjected to transient heat input under conditions designed to minimize thermal stresses, will, in fact, demonstrate the radial and circumferential cracking characteristic of that observed in thermal-reactor fuel elements in steady-state service.* In addition, internal sample transient-pressure buildup due

*Some tendency toward production of such cracking as a result of transient heating is reported in Ref. 2.

to heating of gas contained inside UO_2 pellets has been proposed as a possible mechanism for explosive disintegration of UO_2 fuel under transient heating.(2,3) An ancillary question related to safety is the degree of interaction between UO_2 and cladding as a function of temperature. In general, interaction rates are of interest at temperatures only in the range of the relatively modest coolant temperatures of the present generation of power reactor designs, i.e., ~600°C. In the event of a reactor excursion, however, a "jet" of internal, high-temperature, molten material might escape through a crack in the surrounding rim of oxide and impinge on the cladding,* or coolant might be actually expelled from the reactor core, thus raising cladding temperatures to those typical of the fuel.

The in-pile experimental survey reported here is one undertaken on UO_2 fuel samples as an extension of previous tests in the Transient Reactor Test Facility (TREAT) on metallic, fast-reactor fuel samples.(5-7) Oxide test specimens were "pseudo-EBR-II" elements that were clad with EBR-II cladding thickness, of EBR-II fuel length, and thermally bonded to cladding with inert gas (rather than sodium). Samples were exposed to transient power bursts of the order of 0.5-sec duration, in the absence of coolant, with production of heating rates up to the order of 4000°C/sec. Radial temperature profiles in the fuel during the power bursts were estimated to be comparatively uniform (within ~15%). Cladding temperature lagged behind the fuel temperature, thermal equilibrium between fuel and clad being reached about 2 sec after the peak of the power pulse. Sample cooling was predominantly by thermal radiation.

An inert gas environment was selected for the experiments in order to (1) permit high-speed photography of the samples during the tests; (2) allow use of fast-response cladding thermocouples in measurement of transient temperatures; (3) avoid possible postfailure modification of the sample remains due to presence of liquid-metal coolant; and (4) simplify the experimental conditions that would effect transient thermal stresses in cladding and fuel.

UO_2 was selected as the fuel material rather than mixed UO_2-PuO_2, which would be necessary for an oxide-fueled, fast breeder operating on the U^{238}-Pu^{239} cycle with breeding in the core, to simplify assembly and postexperiment sample inspection. It is believed that results of this survey would be sufficiently general to provide orientation for study of mixed oxide fuels, particularly ones with Pu:U ratios of about 0.15 or less. No specimens previously irradiated to appreciable levels of burnup were used, not only because of the appreciable experimental complexity associated with use of such specimens, but because results of tests with them would be expected to be highly dependent on a variety of additional experimental parameters of design and preirradiation conditions.

---

*A thermal-reactor element failure attributed to this mechanism is reported in Ref. 4.

In addition, large UO_2 and UO_2 fueled-oxide pellets with much different thermal-neutron flux depressions and cladding conditions have been given transient irradiations in TREAT as part of an Argonne research program into metal-water reactions(2) and part of a General Electric Atomic Power Equipment Division development program directed toward use of UO_2-PuO_2 fuel in fast-breeder power reactors.*

*A preliminary account of results being obtained from the GE-APED irradiations of 2.5-cm-diam. UO_2 fuel clad with steel, contained in a heat sink, is given in Ref. 8.

II. EQUIPMENT AND PROCEDURES

A. TREAT

A cutaway view of the TREAT reactor is shown in Fig. 1. TREAT is a graphite-moderated and -reflected, pulsed, engineering test reactor designed and built to meet the needs of the Fast Reactor Safety Program for a versatile facility capable of safely generating a high, time-integrated, neutron flux over a comparatively large sample volume.(9) The reactor engineering design has been reported.(10) Briefly, its core is approximately 120 cm high, with top and bottom reflectors about 60 cm thick. Each fuel element is 10 cm square. Special elements with large slots, nominally 56 cm high by 7 cm wide, can be loaded into the reactor to provide a large core-viewing slot. One such slot is shown in Fig. 1, extending from the flood light to the center of the core.

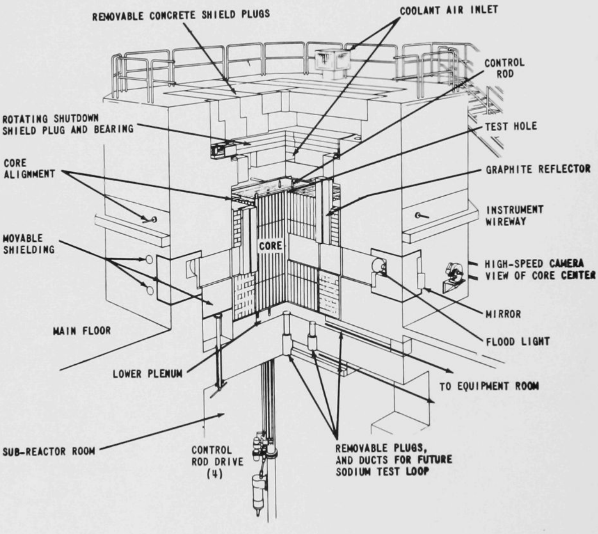

112-771

Fig. 1. TREAT Cutaway

Experimental samples may be exposed in containers designed to fit into the hole left by removal of one or more TREAT fuel elements, or in containers which fit in a core slot. Despite the large perturbations in core neutron-flux distribution caused by the slots and experimental samples, the kinetics analysis(11) that fits the transient behavior of the reactor loaded with a simple solid core(12) was found to fit (with a 10% reduction in the reactor feedback) data for a typical slotted-core loading with a sample.(13)

B. Containers and Samples

The first two series of tests on uranium oxide specimens were run with the experimental samples contained in standard opaque meltdown capsules.[6] The design of the basic capsule, loaded into a Zircaloy well in a special, experimental, dummy TREAT element, is shown in Fig. 2. The steel capsule is lined with a graphite meltdown crucible which holds the sample and contains the sample meltdown products.

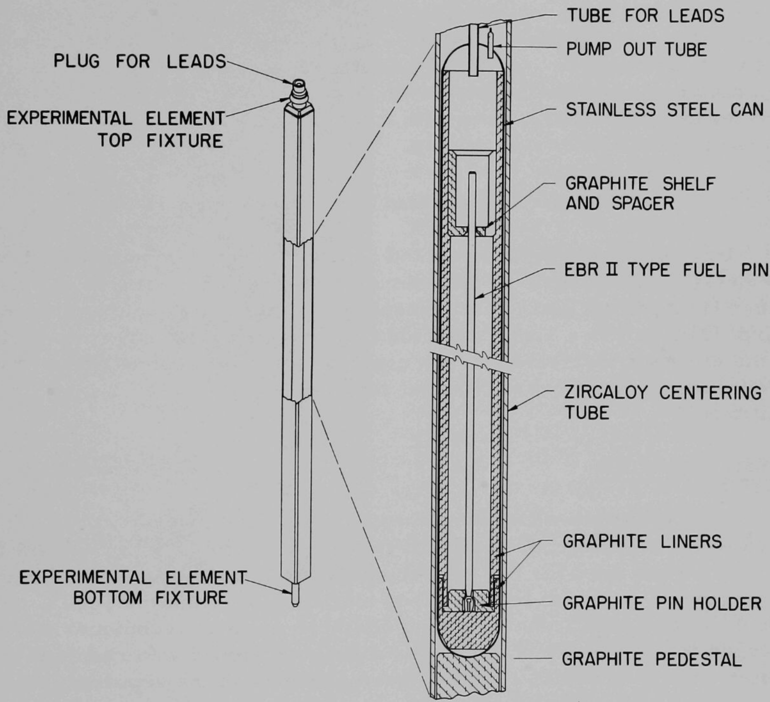

112-2846

Fig. 2. Opaque Meltdown Assembly

Later experiments were performed using the transparent meltdown assembly, and high-speed photography[7] to follow sample transient behavior. This assembly (shown in Fig. 3) has a stainless-steel outer shell which provides a gas-tight containment vessel. The sample is held in a Zircaloy capsule, which is the primary containment. Both the Zircaloy capsule and the steel outer shell have high-purity fused-silica windows.[14]

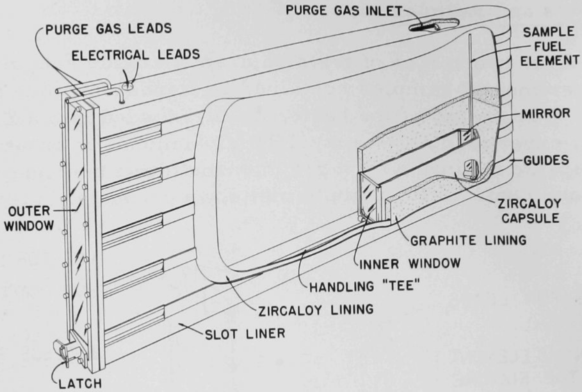

112-1223

Fig. 3. Transparent Meltdown Assembly

Uranium oxide cylinders used in the experiments were made by the ANL Metallurgy division. A cylinder diameter of 0.381 cm was specified because (1) it gave a diametral clearance that permitted convenient assembly and, (2) it fell in a range in which it was determined experimentally that the effective fuel-cladding gap conductance was an insensitive function of clearance, at least over a limited range of steady-state irradiation conditions.(15)

C. Instrumentation

Fuel elements were instrumented with fast-response thermocouples welded to the cladding.(6) Platinum versus platinum-10 w/o rhenium thermocouples were used for the earlier oxide tests, but were not satisfactory for the general program because they melted approximately 1000°C below the fuel melting point. Spot-welding and wire-support techniques were developed to permit use of 0.025-cm-diam. tungsten-5 w/o rhenium versus tungsten-26 w/o rhenium cladding thermocouples in the experiments.

Two tantalum-clad oxide samples were each instrumented with an internal thermocouple and subjected to a succession of transients culminating in one with general fuel melting. The internal thermocouples were 0.15-cm-diam., thoria-insulated, tantalum-clad, tungsten-5 w/o rhenium versus tungsten-26 w/o rhenium units with junctions welded into the sheath tips. The thermocouples were inserted into short, close-fitting holes drilled along the axis of uranium oxide cylinders. To promote consistent contact between the ceramic fuel and the sheathed thermocouple, each thermocouple was located at the bottom of the element, and the stack of oxide cylinders above was spring-loaded by means of a rhenium spring between the tantalum top plug and the top of the oxide column. Figure 4 is a radiograph of this element instrumentation arrangement, with the elements turned so the thermocouples are at the top. This thermocouple and void can produce a large perturbation.

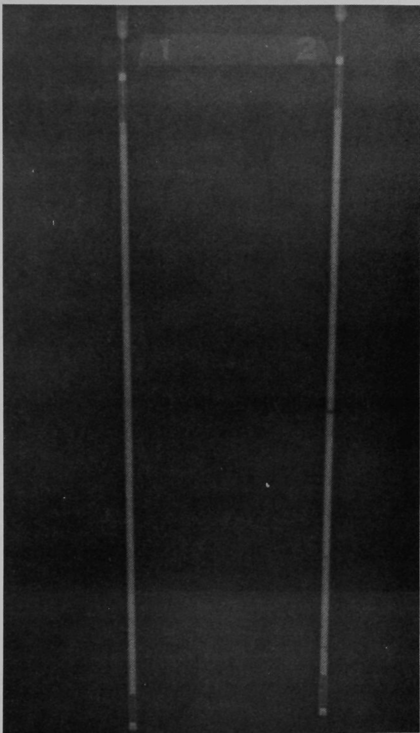

112-2547

Fig. 4. Radiograph of Tantalum-clad Oxide Samples with Internal Thermocouples

Tantalum was selected as the sheath material over such possible competitors as molybdenum, niobium, tungsten, and tungsten-26 w/o rhenium alloy because of its high melting point, availability, and comparatively good mechanical properties. Compatibility with UO_2 was expected to be acceptable; it has been reported that fused UO_2 powder placed in contact with commercially pure tantalum, and heated to 2660°C for one hour, produced no penetration of the metal.[16] Thoria was specified as the insulator because of its comparatively high electrical resistance at elevated temperatures. One review gives a value for thoria resistivity of 1×10^4 ohm-cm at 2050°C, compared with 8×10^2 ohm-cm for beryllium oxide at 2100°C, and 1 ohm-cm for ZrO_2 at 2000°C.[17] Kerr[18] reports no reaction between thoria and tantalum up to 2795°C, or between thoria and tungsten up to 2645°C.

The behavior of these two thermocouples was consistent. Figure 5 is a graph of maximum internal temperatures measured with these thermocouples, as a function of reactor integrated power for the transients in which they were used. The delay between the reactor power pulse and the temperature output was larger than that for the fast-response cladding thermocouples. Figure 6 is a graph comparing temperature data from an internal thermocouple with data from a typical cladding thermocouple (not opposite the internal thermocouple). The internal thermocouple displays a transient temperature "peak" well above the cladding maximum temperature, but shows lower temperatures during cooling than that of the cladding. This was a consistent effect: it is believed to be real, and to be due to replacement of fuel by the heat-absorbing sheath and insulation. The heat-transfer phenomena for the sheathed thermocouple should be similar to those for the cladding, but the greater heat absorption in the thermocouple compared with that of the cladding would produce slower internal-thermocouple temperature rise and greater temperature depression. The temperatures recorded from cladding thermocouples at the same axial position as the internal thermocouples were consistently low, in agreement with the low cooling temperatures from the internal thermocouples.

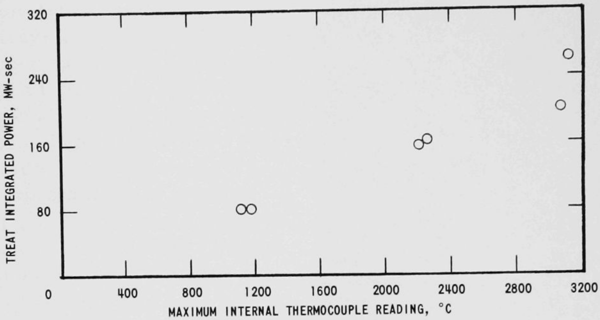

Fig. 5. Maximum Internal Sample Temperatures Measured by Internal Thermocouples

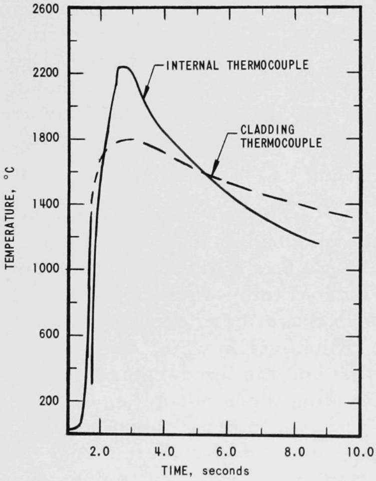

Fig. 6

Comparison of Cladding and Internal-thermocouple Transient Data

An attempt at SPERT I has been reported(19) to produce and use an internal thermocouple consisting of two bare thermocouple wires welded together to form one long wire with the junction located in the middle of the uranium oxide. This device uses the UO_2 itself as the insulator, and has a minimum mass. The SPERT fuel rod was made with powdered oxide and was used in a water environment. A similar device would be quite difficult to design and operate in a sodium environment, although it would have been ideal for the transient tests reported herein. An attempt(20) was made to fabricate UO_2 cylinders of diameter larger than those in the EBR-II size cladding, containing tungsten-5 w/o rhenium versus tungsten-26 w/o rhenium thermocouples made by welding pairs of 0.025-cm-diam. wires together to form a single wire from each pair. Small holes about 50% larger in diameter than the wires were drilled in the "green," or unfired, ceramic material, and thermocouples inserted so that the junctions were located on the cylinder axes. The cylinders were then fired. The refractory metal wires, however, became brittle during the sintering, and those wires that did not break off at the surface of the cylinder during removal from the sintering furnace broke during subsequent handling.

Results have been reported of a detailed testing program(21) evaluating somewhat similar 0.15-cm-diam. tantalum-sheathed tungsten versus tungsten-26 w/o rhenium thermocouples with beryllium oxide or magnesium oxide insulation for steady-state use in BORAX-V fuel rods. Beryllium oxide was selected as the better high-temperature material, but a maximum temperature limit of approximately 2200°C was established even for the beryllium oxide, because of the reaction observed between the beryllium oxide and the tantalum.

D. Procedures

1. Reactor Settings. Experimental reactor settings were specified on the basis of a previously obtained calibration between sample energy input for metallic EBR-II specimens and reactor integrated power, and calculated sample flux-depression factors.(6) Time and space dependences of sample temperatures were estimated using the CYCLOPS transient heat transfer code,(22) standard values of material properties, and a value of 0.2 Watt/(cm^2)(°C) for the thermal conductance of the gap between fuel and cladding.(15) Because of limitations in the code, the gap conductance was lumped with the cladding physical properties. Because of the low oxide conductivity and low gap conductance, the peak fuel temperature along the axis was found to be essentially that given by calculations of isothermal adiabatic energy input to the fuel alone, and the peak cladding temperature was calculated to be found about 2 sec after the power pulse.

Settings for transient experiments subsequent to the first series of excursions were made on the basis of experimental temperature data, which were corrected as necessary for different relative thermal-neutron flux changes caused by changing sample capsules or sample claddings.

2. Inspections. After exposure of a sample in TREAT, it was shipped to hot-laboratory facilities at the Argonne site for postmortem

examination. The activity level, at this time, normally did not exceed 200 or 300 mR/hr at 2 in. from the sample. This permitted inspection without employing remote handling techniques. Thus, all work was accomplished by limiting the exposure time of the operator working through a shielded (~3 in. of lead) glovebox.

A portable power saw was used for cutting off the tops of the dry opaque capsules. This permitted easy removal of the graphite crucibles and the test fuel element for further inspection.

Where possible, the inspection covered the following items:

(1) The cladding was closely examined for penetrations. Uncoiling of the spacer wires, if any, and distortion or warping of the sample element were noted.

(2) After removal of the cladding, its inner surface was inspected for evidence of any oxide-cladding reaction zones. In some cases, cross sections of the cladding were taken and mounted for metallographic observation.

(3) The oxide slugs were measured for growth in the radial direction. Changes in length and number of slugs due to breakdown of the original longer lengths were recorded. Measurements were made to determine change in density. Where the transients resulted in extensive breakdown of the oxide slugs, particle size distribution was determined.

(4) During the inspection, photographs were taken, for record, of certain phases that were of particular interest. In some cases, samples of the oxide were submitted for burnup analysis as a recheck on earlier power-calibration runs.

III. EXPERIMENTAL RESULTS

A. Experimental Conditions

Five series of experiments were conducted using oxide (UO_2) fuel. For the first two series, the opaque type,(6) inert-gas-filled capsules were used. The transparent type capsule(14) was used for the other three series.

The five series are identified as follows, along with a brief statement about the purpose of the series:

SXXII	Survey of possible meltdown or significant premeltdown fuel behavior.
SXXV	Effects of cycling and use of refractory metal cladding.
SXXVIII	First transparent (photographed) meltdown study on UO_2 fuel samples.
SXXXII	Study of oxide-sample transient behavior at higher temperatures.
SXXXIII	Continuation of higher-temperature, oxide-sample transient-behavior study.

The results of the oxide series conducted up to the present are summarized in Table I, to provide orientation for the following sections on photographic and postmortem results. Sample energy values were not measured directly; they are estimates based on prior reactor calibration and calculated flux-depression factors.

B. Photographic Results

The first photographic records of oxide sample failure came from stainless-steel-clad specimens 2 and 3 of the third oxide series (XXVIII). Failure was nonviolent, and occurred just before cladding melted. Figure 7 consists of still black-and-white prints taken from the color film of the failure of sample 3 of Series XXVIII. Figure 7A shows the specimen intact at the beginning of the reactor transient; the element, proper, is at the left, and its image appears at the right in a mirror located at the end of the Zircaloy capsule. Figure 7B shows the element after the reactor excursion was over at the time of failure. The triangular dark patch near the center is attributed to "charring" of the plastic paint in the powdered alumina-white paint mixture that is used to coat the capsule walls to provide a diffuse white background for the photography.* This blackening could

*Preliminary analysis of the photographs resulted in the conclusion that this patch was a dark cloud (probably powdered oxide) emitted from the sample upon failure. However, more detailed study of the photographs of the sample and the mirror image showed that the patch appeared on the wall, not in front of it. This does not preclude emission of a small amount of powdered oxide, but does show that any amount ejected was not directly visible.

Table I

SUMMARY OF MELTDOWN EXPERIMENTS WITH UO_2 SAMPLES

Test	No.	Cladding	Spacer Wires	Integrated Reactor Power (MW-sec)	Estimated Sample Energy Input (cal/gm)	Initial Reactor Period (msec)	Max. Recorded Cladding Temperature (°C)	Remarks
SXXII	1	SS	No	46 350	110 840	270 150	660 1590	
	2	SS	No	46	110	270	895	No damage to fuel or cladding
	3	SS	No	71	170	270	1162	No damage to fuel or cladding
	4	SS	No	97	233	270	1340	Complete meltdown of cladding
	5	SS	No	132	317	270	1625	Fuel condition altered
SXXV	1	SS	Yes	44 44 44	106 106 106	270 270 270	746 742 790	Cladding intact, samples warped, some fragmentation of fuel
	2	SS	Yes	62 62 62	149 149 149	270 270 270	970 1017 1010	Cladding intact, samples warped, some fragmentation of fuel
	3	Ta	No	91	206	270	1570	No damage to fuel or cladding
	4	Ta	No	124	280	270	1740	Cladding intact, fuel altered
SXXVIII	1	SS	Yes	72	144	150	1125	Sample badly warped
	2	SS	No	132	264	150	1813	Total cladding failure
	3	SS	No	176	352	150	1435	Total cladding failure, void and fissure in fuel
	4	Ta	No	117 117 117	220 220 220	150 150 150	1480 1660 1660	Cladding undamaged, fuel unchanged
	5	Ta	No	176	331	150	1660	Cladding intact, complete fragmentation of fuel
SXXXII	1	Nb	No	123	248	125	2140	Sample slightly warped
	2	Nb	No	172	347	125	2310	Small hole in cladding
	3	Ta	No	85 132 185 225	160 248 348 423	125 125 125 125	1160 1780 2330 2330	Bulge in cladding, oxide fragmented upon removal
	4	Ta	No	275	517	125	2690	Cladding destroyed, oxide fragmented
SXXXIII	1	Nb	No	175	354	100	2200	Sample warped, no cladding failure; oxide contains voids and melted centers
	2	Nb	No	200	404	100	2260	
	3	Ta	No	85 142 200	160 267 376	100 100 100	1140 1883 2400	
	4	Ta	No	85 142 275	160 267 517	100 100 100	1150 1820 2460	Cladding destroyed; oxide fuel reduced to mass of fragments

A B C D E

112-2753

Fig. 7

Photographs of Failure of Stainless-steel-clad Oxide Sample Subjected to 176-MW-sec Transient

have been caused by a sudden expulsion of hot gas from the cladding upon failure. Figures 6C, 7D, and 7E show individual frames from the subsequent collapse of the sample under the influence of gravity as the cladding temperature reached the melting point.

By contrast, Fig. 8 is a still print from the film of the experiment on sample 5 (Series XXVIII), which was tantalum-clad and given a TREAT burst equal to that for sample 3 shown in Fig. 7.* Figure 8 is typical of the appearance of that specimen at, or near, its maximum cladding temperature. As before, the sample is on the left, and the mirror image is on the right. The dark "stalks" are

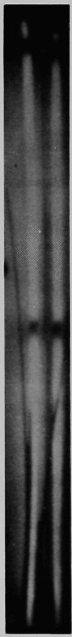

112-2752

Fig. 8

Appearance of Tantalum-clad Oxide Sample Subjected to 176-MW-sec Transient

*Because of different neutron absorption, the sample 5 energy input was about 6% less than that of sample 3.

alumina tubes used to insulate and support platinum and platinum-10 w/o rhenium thermocouple wires, originally welded to the cladding, but which became detached during the experiment as the cladding approached the melting points of the wires. Two cold segments are visible along the sample. Since the oxide cylinders were not constrained from axial movement inside the cladding, the stack of cylinders could be jarred sufficiently during postassembly handling and shipment so that individual cylinders could be shifted in position and canted, thus opening up axial gaps. The length of hot sections was the same, within accuracy of determination, as the length of oxide originally loaded in the tubing.

More dramatic is the failure of a tantalum-clad oxide sample (sample 4 of Series XXXIII), which is depicted in Fig. 9, with the emission of molten UO_2 and disintegration of molten or near-molten cladding. The figure traces the course of the test from heating of the tantalum tube, through the failure with expulsion of molten oxide.* Meltdown fragments

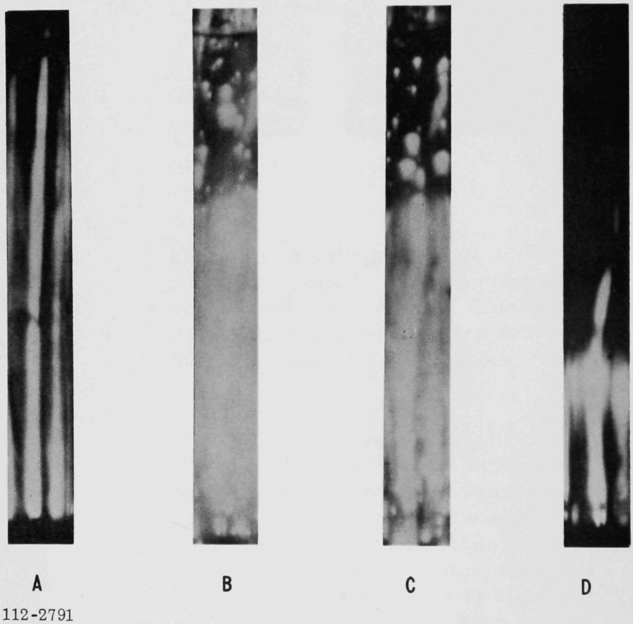

Fig. 9. Photographs of Failure of Tantalum-clad Oxide Sample

*Multiple reflections are visible around the sample on the capsule walls, which were not coated with the nonglare, white paint (customarily placed on the walls to suppress reflections), so that smoke from thermally-decomposing paint would not obscure the behavior of the high-temperature samples.

were observed, from the film, to fly from the location of the element. Velocities ranged from 150 to 290 cm/sec for particles moving upward. Some others, "rebounding" from the lower part of the capsule, had velocities in the range of 106 to 220 cm/sec. The internal thermocouple output for this transient was quite erratic and ended approximately 100 msec after failure began.

C. Postmortem Results

1. Series XXII Dry Opaque (Five Samples)

a. Sample 1. Meltdown of the lower 2 cm of the cladding occurred. The oxide fuel vaporized. No indication of violent rupture of the cladding or "explosive" failure occurred. (The sample was a minature specimen run to vaporization to test for possible hazards in the experiments.) See Fig. 10.

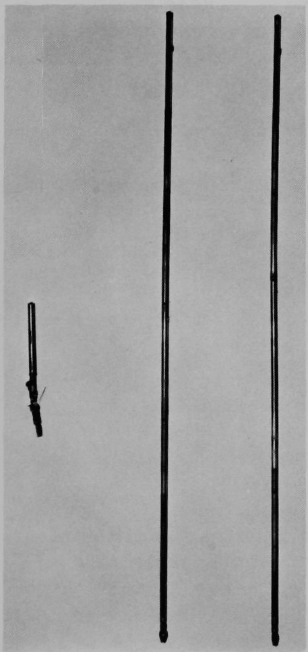

112-1025

Fig. 10

Series XXII Samples 1, 2, and 3 (left to right) Stainless-steel Clad, without Spacer Wires

b. Samples 2 and 3. No warpage occurred. The cladding discolored along several short zones between the upper and lower 6 cm of the samples due to localized heating. There was no dimensional change in cladding. Figure 10 shows the condition of samples 1, 2, and 3 as removed from the opaque capsules. Note that samples 2 and 3 had the spacer wires removed before testing. The oxide fuel showed no surface cracks or evidence of melting along the axial center of the slugs. Dimensional checks showed no radial or axial growth. Microscopic examination of oxide from samples 2 and 3 showed the same structure as an unexposed control-fuel specimen.

c. Samples 4 and 5. Almost complete meltdown of the cladding occurred except for the top and bottom sections. All oxide slugs were broken down to shorter lengths. Approximately 40% of the slugs removed from sample 5 had deep cracks radiating outward from the center of the slug. The cladding from sample 4 had a rupture zone ~1 cm long located between 8 and 9 cm from the top of the sample. This zone is clearly shown in Fig. 11. Cracks can also be seen in the oxide cylinders from sample 5. Note the uniform spacing of the unmelted cladding on both samples. There was no evidence of an oxide-cladding reaction. Pieces from samples 4 and 5 contained fissures and central cylindrical regions of marked difference in appearance from the control. These regions, extending through the entire length of the cylinders, were composed of large, loosely bonded, crystal-like particles of oxide surrounded by the remaining sleeve-shaped section of the original oxide slug.

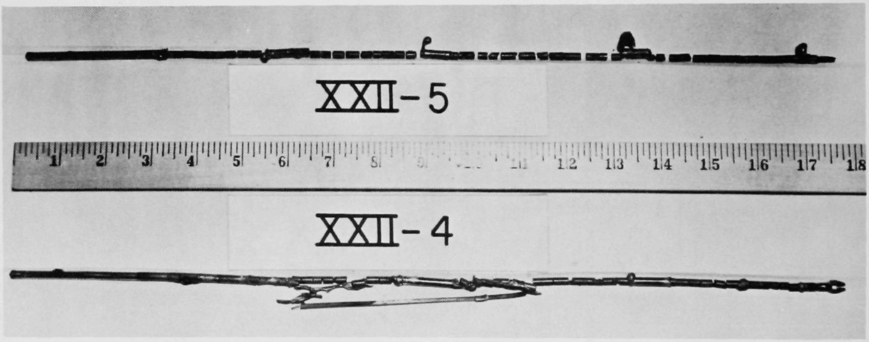

112-1058-A

Fig. 11. Series XXII Failed Samples 4 and 5 Showing Condition of Materials as Recovered from Irradiation Capsule

2. Series XXV Dry Opaque (Four Samples). No evidence of cladding failure occurred in any of the specimens. The spacer wires on samples 1 and 2, by uncoiling, produced extensive twisting and warping of the elements with consequent local fragmentation of the oxide. The extent of fragmentation is shown in Fig. 12. Samples 3 and 4, although not warped, contained about the same amount of fuel fragments, plus some fines or oxide dust (see Fig. 13). Microscopic examination showed the oxide from samples 1, 2, and 3 to be unchanged or like the unirradiated

control material. Oxide from sample 4 had the "recrystallized" central regions, as described above for samples 4 and 5 of Series XXII.

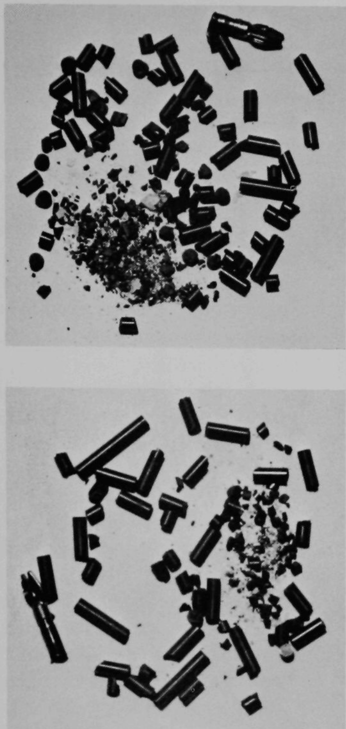

112-1194

Fig. 12. Series XXV Fragmented Oxide from Samples 1 (top) and 2 (bottom)

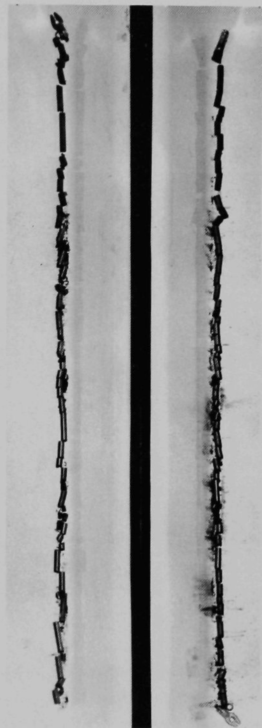

112-1195

Fig. 13. Series XXV Samples 3 and 4 (left to right) Showing Fuel after Removal of Tantalum Cladding

3. Series XXVIII Dry Transparent (Five Samples). Figure 14 shows all five samples of Series XXVIII as removed from the capsules. The fuel recovered from capsules 2 and 3 was laid out, as shown, merely for the purpose of photographing. Figure 14 does not represent the position each piece occupied in the sample before irradiation. Contrast sample 1 of this series, having spacer wires attached to the cladding, with sample 3 in Fig. 10. Note the spot on sample 5, ~15 cm above the spade. The spot appeared as though the clad had almost reached its melting point and some of the material had started to flow. However, estimated

maximum cladding temperature (2050°C) is considerably lower than the melting point of tantalum. The spot was probably produced by an alumina tube used to insulate the cladding thermocouple. (See Series XXXII discussion in par. 4 below.)

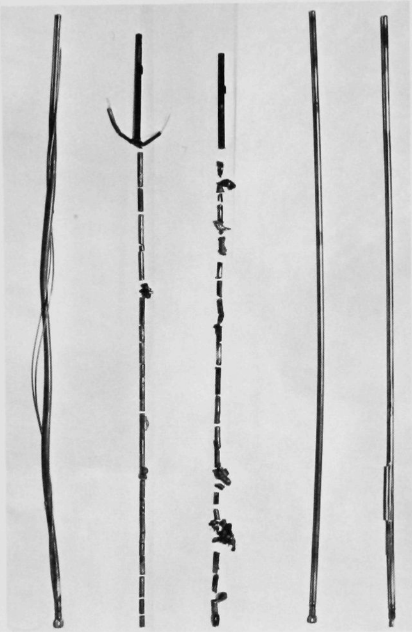

112-1415

Fig. 14. Series XXVIII Samples 1 through 5 (left to right) Showing Complete Failure of Samples 2 and 3

a. Sample 1. The spacer wire uncoiled, and the sample was badly warped but no failure or penetration of the cladding occurred. The original loading consisted of nine oxide slugs, each ~4 cm long. After the transient test, 49 slugs were removed. Approximately 88% of these measured ~0.5 cm. Neither increases in diameter nor chips or fragmentation were found.

b. Sample 2. All but the upper 8 cm of the cladding completely melted. All oxide was accounted for, and there was no indication of an oxide-cladding reaction. The original loading of nine oxide slugs fragmented to 23 slugs after the transient test; 45% of these measured between 1.0 and 1.5 cm. Microscopic examination of the oxide showed the typical "recrystallized" central region.

c. Sample 3. The cladding was destroyed to the same extent as that found with sample 2. The length of the oxide slugs was reduced to ~1 cm. Approximately 50% of the slugs were found to be tubular, having a central void (0.12 cm) extending through the slug.

d. Samples 4 and 5. The cladding (tantalum) on sample 4 remained intact. Practically no warpage or distortion occurred. On sample 5, a small cladding rupture was found about 15 cm above bottom. Oxide slugs in sample 4 were broken into shorter lengths, but there was no indication of melting or structural change. The oxide slugs in sample 5 were found to be completely granulated into pieces from about 0.1 to 0.3 cm in length. Fines and dust amounted to 3 to 5% of the total fuel weight.

4. Series XXXII Dry Transparent (Four Samples). The postirradiation condition of the two niobium-clad (1 and 2) and two tantalum-clad (3 and 4) samples is shown in Fig. 15. The dark material adhering to samples 1, 2, and 3 is vitrious alumina thermocouple insulation, which became solidly fused to the cladding during the transient test. Alumina melts at 2015°C.[17]

112-1933

Fig. 15. Refractory-metal-clad Samples 1 through 4 (left to right) of Series XXXII

a. Sample 1. The sample was intact and slightly warped, and the cladding extremely brittle. The outside diameter of the cladding increased by 0.002 to 0.005 cm. The oxide cylinders showed typical diameter increases of 0.002 to 0.005 cm, for both sample 1 and sample 2.

b. Sample 2. The sample was slightly warped. A small hole was found in the cladding at a point 22 cm from the bottom. The cladding diameter increased by about 0.005 to 0.008 cm. From the rise in activity recorded at the fission gas trap in the capsule-cover gas system, it was concluded that the hole was produced during the transient test. Fuel slugs from samples 1 and 2 took either the form of a loosely bonded oxide core surrounded by a harder cylinder, comparable in appearance with unexposed oxide, or hollow (or partially hollow) cylinders with a hard, fused, inner surface. An end view of the material from samples 1 and 2 is shown in Fig. 16. Note the tendency toward a concave surface on the ends of the cylinders. This occurred not only for the "broken" ends, but for the original, machined ends also. The maximum fuel temperature estimated for sample 1 was about 2700°C; center melting should have occurred in sample 2. Figure 17 shows the relatively unchanged outer surface of the same oxide fuel shown in Fig. 15. Note the short lengths of postirradiation oxide, and the two well-formed solidified drops of oxide near the top, and one-fourth of the way from the top of sample 2.

c. Samples 3 and 4. The cladding on sample 3 was intact, but a section between 10 and 20 cm from the bottom was bulged to about 4.75-mm diameter. The cladding on sample 4 showed that extensive melting had occurred along a zone between 8 and 17 cm from the top. Fuel cylinders from both samples were similar in appearance to those from samples 1 and 2. They appeared to adhere slightly to the inner wall of the cladding. Removing the fuel cylinders resulted in their breaking down into a mass of chips and granules with no fuel remaining permanently fixed to the inner wall of the cladding. Neither the oxide fragments nor the inside of the cladding showed evidence of a fuel-tantalum interaction zone, however, upon subsequent inspection. Figure 18 shows sample 4 still contained in the Zircaloy inner liner of the "transparent" capsule. The view is taken from the back end of the capsule liner through the opening normally covered or occupied by a quartz mirror. The discolored surface of the inner liner, opposite the point where the sample melted, indicates the intense heating that the liner was subjected to in that area. However, this particular inner-liner design has proved to be more than adequate for all experiments conducted to date.

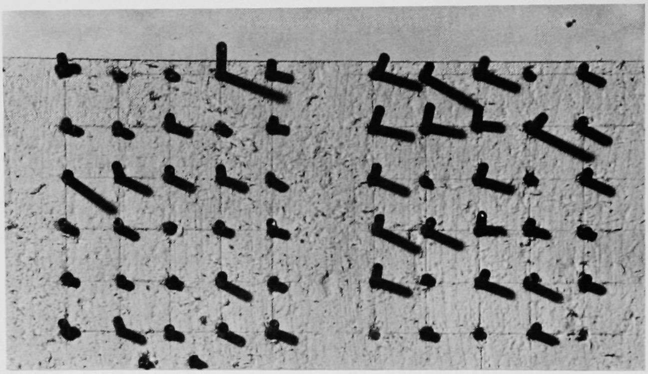

112-1936

Fig. 16. Oxide Slugs from Samples 1 and 2 (left to right) of Series XXXII, End View with Oblique Lighting Showing Hollow Slugs and "Recrystallized" Centers

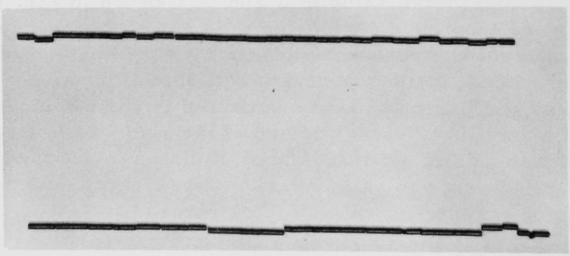

112-1935

Fig. 17. Oxide Fuel Slugs from Samples 1 and 2 (top to bottom) of Series XXXII after Removal of Niobium Cladding

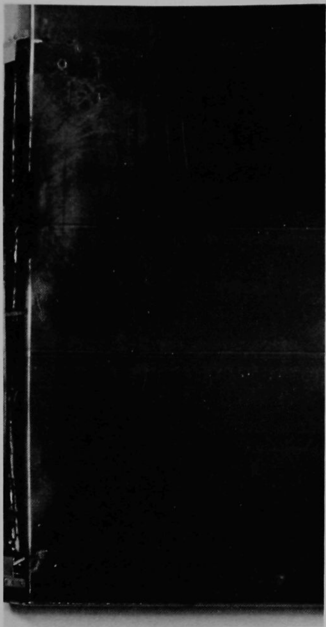

112-1934

Fig. 18. Sample 4 of Series XXXII Contained in Zircaloy Inner Liner of Transparent Irradiation Capsule

5. Series XXXIII Dry Transparent (Four Samples). The posttransient condition of the four refractory-metal-clad samples of Series XXXIII are shown in Fig. 19. The tantalum-sheathed tungsten-rhenium "internal" thermocouples are shown, still attached to the tantalum-clad samples. Figure 20 shows the fuel after being removed from the cladding. The ends of the internal thermocouples are also shown here. Microscopic examination revealed that the tips of the sheaths of both thermocouples were melted away (that of sample 4 being much worse than that of sample 3).

a. Samples 1, 2, and 3. The samples warped slightly, but the cladding did not fail. Concave cylinder ends were common. A trace of thin, loose surface scale appeared on the bottom 2 cm of the cladding of pins 1 and 2. The cladding from samples 1 and 2 was found to have expanded to about 4.83 mm diam. The cladding diameter increase for sample 3 was about 0.012 cm. The appearance of the individual fuel cylinders, from these samples, was similar to that found in other specimens reaching temperatures above 1600°C. There was no evidence of metal-oxide reaction zones. There was no fragmentation, other than the oxide slugs breaking down from lengths of ~3.4 cm to lengths of 0.8 cm.

b. Sample 4. Cladding failure was extensive along the entire upper 16 cm of the sample. All fuel, with the exception of one piece about 0.8 cm long, was ejected from the cladding. The cladding outside diameter was found to have increased by about 0.016 cm. Metallographic examination of cladding from the melted section failed to reveal anything that could be identified as a tantalum-uranium oxide diffusion or interaction zone. Figure 21 is a photomicrograph of tantalum cladding taken from a section adjacent to the point of failure. The large crystal grain boundaries throughout the section are indicative of extremely high-temperature conditions, and the slightly irregular, pitted inner edge of the clad could be taken to indicate that the temperature of the inner surface had reached the melting point of tantalum (~3000°C). All the fuel recovered from the transparent capsule is shown in Fig. 22. About half the material appeared to be in the form of coarse granules. The remainder consisted of thick shell-like fragments that might have resulted from the breakdown of hollow cylindrical sections, described in connection with Series XXXII. A typical particle-size distribution of the material remaining after complete destruction of the original oxide cylinders is shown in Table II.

112-2123

Fig. 19

Series XXXIII Samples 1 through 4 (left to right) Showing Internal Thermocouples and Extent of Warpage

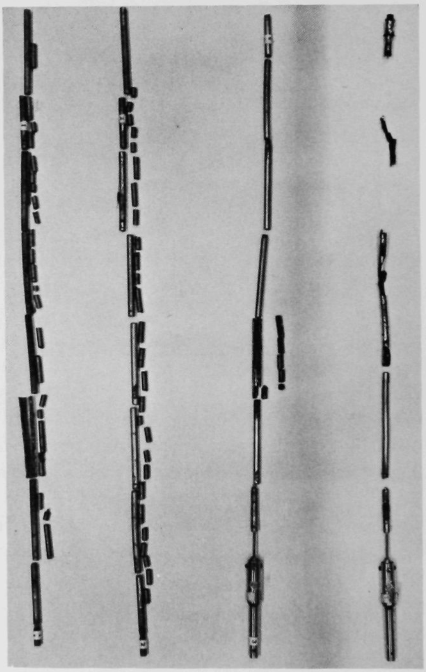

112-2144

Fig. 20

Series XXXIII Showing Oxide Fuel from Samples 1 through 3 and the Melted Tip of the Thermocouples in Samples 3 and 4 (Same Orientation as Fig. 19)

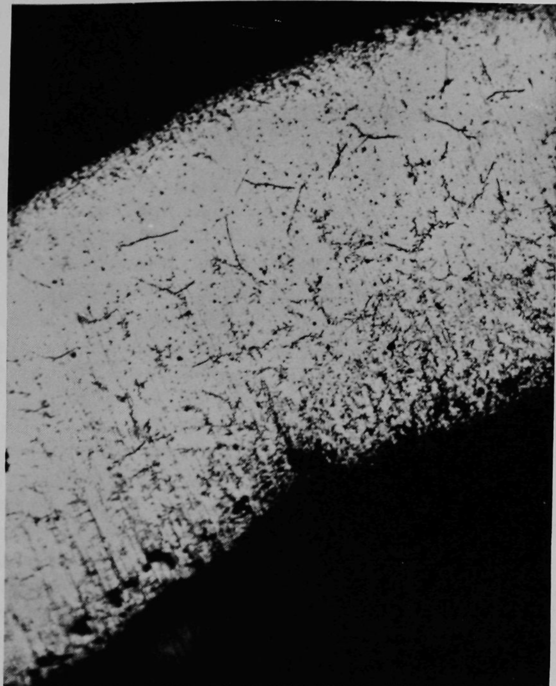

112-2375

Fig. 21. Series XXXIII Sample 4, Photomicrograph of Tantalum Cladding from Section near Point of Failure

Fig. 22

Series XXXIII Sample 4, Condition of Oxide Recovered from Inner Liner after Failure of Sample

112-2122

Table II

PARTICLE-SIZE DISTRIBUTION OF UO_2 FUEL CYLINDERS AFTER FAILURE OF REFRACTORY METAL CLADDING

SXXXIII, Sample 4

Size Range (microns)	Per Cent of Total Sample
0-148	2.0
149-249	2.7
250-419	8.2
420-839	35.9
≥840	51.1

c. Density Changes. Several oxide cylinders from samples 1-3 of Series XXXIII were taken for density measurements to check the apparent density increase indicated by the concave ends. The material selected was from the elements that exhibited a recrystallized or glassy center zone. Maximum central fuel temperature was estimated to range from about 2700°C through melting. Table III is a summary of the data on five of these specimens, which showed an average postirradiation density of 95.6%.

Table III

DENSITY OF SPECIMENS GIVEN HIGH-TEMPERATURE EXPOSURE

Specimen No.	Density (gm/cc)	Per Cent of Theoretical
1	10.482	95.5
2	10.203	93.0
3	10.758	98.1
4	10.114	92.2
5	10.857	99.0

The density of the oxide used (preirradiated) for the experiments covered in Table III was 93.0% of theoretical.

IV. ANALYSIS

A. Temperature Calculations

Transient sample temperatures were calculated for the experiments in order to obtain the radial temperature variations throughout the transient heating and cooling. From these calculations, estimates could be made of thermal stresses in the fuel and the cladding, and effective values of the heat-transfer coefficient between the fuel and the cladding. Computed "estimates" of the transient temperature history of the sample interior could be made for a given experimental curve of transient cladding temperature. Effects were studied for two types of cladding: steel and tantalum. Tantalum results were assumed to be typical of those for niobium cladding because both metals have nearly equal values of thermal conductivity, k, and specific heat per unit volume, ρ Cp. Transient temperature calculations were made using the Argonne IBM-704 transient heat-transfer code RE-248 ARGUS,[23] which is a newer and more powerful version of the RE-147 CYCLOPS code used earlier.[6] The newer code is used for these calculations because it permits explicit use of a boundary conductance, U (like that between the UO_2 fuel and metal cladding), without "lumping" the U into an effective thermal conductivity for an adjacent material region, and because the cladding region can be used as a separate region in the calculations without forcing computations to use an excessively large number of iterations for mathematical convergence. Material property values used are listed in Table IV.

Table IV

MATERIAL PROPERTY VALUES USED IN TRANSIENT TEMPERATURE CALCULATIONS

Material	Thermal Conductivity, k [W/(cm)(°C)]	Specific Heat per Unit Volume, ρ Cp [W-sec/(cc)(°C)]
Uranium oxide fuel	0.0211	3.34
304 stainless steel	0.25	5
Tantalum	0.6285	2.615

The value of oxide thermal conductivity given in Table IV was selected as typical for $UO_{2.04}$ of about 90% density over the temperature range above 1000°C, on the basis of reported results over the range of 833 to 2112°C,[24] and over the range of 800 to 1150°C.[25] No provision was made for a large increase in thermal conductivity at temperatures above 1500°C as reported from postirradiation examinations and calculations of radiant heat-transfer enhancement at high temperatures.[26] The tantalum thermal conductivity value was adopted from a literature survey,[27] and the tantalum value for ρ Cp was an average, over the temperature range of interest, obtained from measurements of tantalum Cp at elevated temperatures.[28]

ARGUS, like CYCLOPS, computes transient temperatures resulting from a transient power input per unit volume of fuel, $P(r,Z,\tau)$ at radius r, axial position Z, and time, τ, given by the equation

$$P(r,Z,\tau) = \theta_0\ \mu(r)\ \eta(Z),\ n(\tau), \tag{1}$$

where μ, η, and n are arbitrary numerical functions given pointwise for r, Z, and τ, respectively. Since no axial power variation was built into the experiments, $\eta(Z) \equiv 1$. Values of relative radial power were calculated using a semiempirical relationship given by Taraba and Paine.[29] This relationship has been found to agree well with results of calculations of radial thermal-neutron flux, that were made using the SNG approximation to the transport equation, spanning the sample values of macroscopic thermal-neutron absorption and outer radius. Table V presents the relative radial-power values averaged over the calculation regions, $\mu(r)$, used in the calculations. (Values were normalized so that power at the outer surface would be unity.)

Table V

AVERAGED RELATIVE RADIAL-POWER VALUES USED IN TRANSIENT TEMPERATURE CALCULATIONS

Outer Radius of Region (cm)	Relative Radial-power Value, $\mu(r)$
0.01905	0.8286
0.05715	0.8331
0.09525	0.8521
0.13335	0.8819
0.16145	0.9293
0.1905	0.9647

Values of the effective heat-transfer coefficient, h, for the outer surface of the cladding were obtained by measuring the rates of temperature drop recorded by the sample cladding thermocouples. Figure 23 is a graph of the heat content, referred to 25°C, of Type 304 stainless-steel-, niobium-, and tantalum-clad oxide samples. Within the accuracy of plotting the data of the figure, the curves for niobium- and tantalum-clad samples

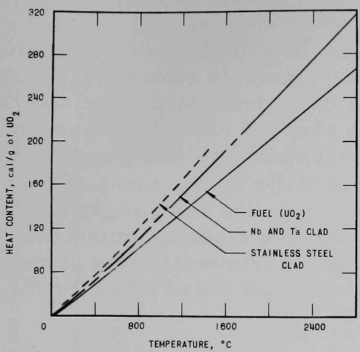

Fig. 23. Isothermal Sample Heat Content as a Function of Temperature

coincide. Data for UO_2 were taken from Belle's computation[30] for steel from standard sources, and for niobium and tantalum from Ref. 28. Values of heat transfer were obtained as a function of temperature from the cooling curve for each thermocouple record trace as follows: First, a convenient increment of temperature (of the order of 150°C) was selected. The corresponding increment in time, $\Delta\tau$, was selected. The heat lost, ΔH, due to the drop in temperature was read directly from Fig. 23. The resulting value of $\Delta H/\Delta\tau$ was divided by the cladding surface area per gram of fuel. This procedure, although based on a model of an isothermal cooling body, is rigorous if two conditions are met: (1) $\Delta\tau$ is small enough so that the temperature loss throughout the body is uniform, and (2) material ρ Cp over the actual temperature distribution is equal to that at the surface temperature. Both conditions are satisfied for these experiments, within the accuracy of measurement.

Five cases were considered: tantalum- and steel-clad specimens in the opaque containers, and samples with all three claddings in transparent containers. Figure 24 shows the experimental heat transfer for

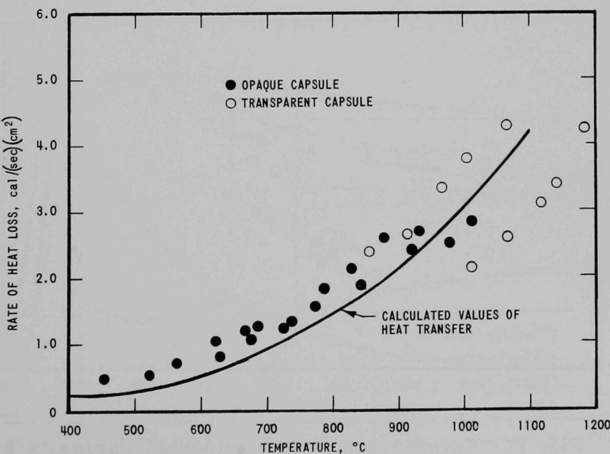

Fig. 24. Comparison of Experimental Values of h with Those Calculated for Radiant Heat Transfer for Stainless-steel-clad Samples

steel-clad specimens in both types of containers. No experimentally significant difference was noted between behavior in each capsule. Figure 25 displays data taken from the experiments with tantalum-clad samples run in opaque and transparent containers. Again no experimentally significant difference was observed for the two cases. Figure 26 contains data points for runs made on niobium-clad specimens in the transparent containers. For comparison, Figs. 24, 25, and 26 also show values of heat transfer for sample heat loss calculated with the assumption of heat transfer only by thermal radiation to the high-reflectance walls of the transparent capsule. Calculated heat losses for the opaque capsules were slightly higher, but were well within the uncertainties in effective cladding emissivities. From these comparisons, it is seen that the experimental rates of heat loss are in reasonable agreement (~±30%) with calculated rates for the higher temperatures of interest.

An important value for calculations, which is believed to be not amenable to calculation, is the effective boundary conductance, U, between fuel and cladding. However, the shape of the heating and cooling curve for the cladding depends upon competition between heat transfer through and from the fuel, and the loss to the sample surroundings. Given the sample energy input, relevant material properties, and the effective heat-transfer coefficient h, one may calculate a family of cladding

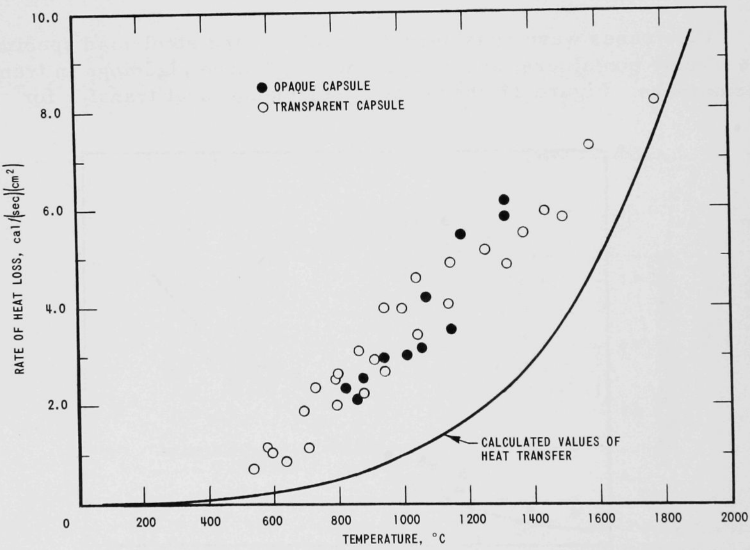

Fig. 25. Comparison of Experimental Values of h with Those Calculated for Radiant Heat Transfer for Tantalum-clad Samples

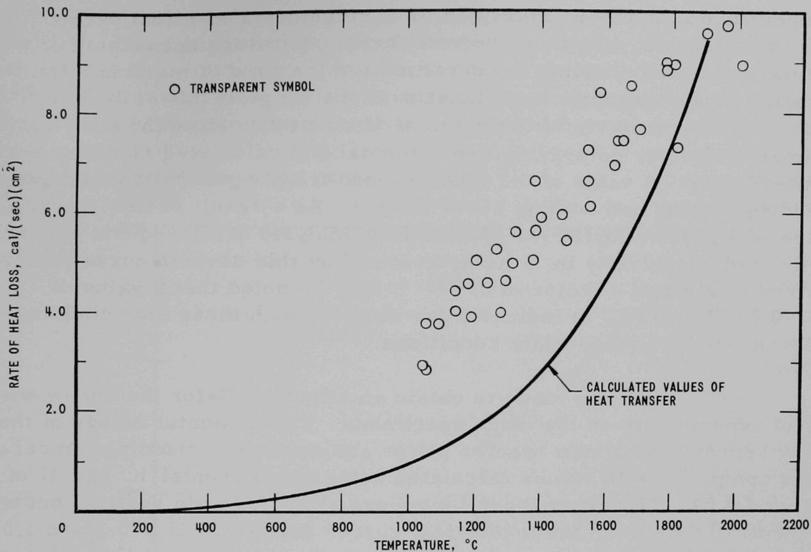

Fig. 26. Comparison of Experimental Values of h with Those Calculated for Radiant Heat Transfer for Niobium-clad Samples

temperature curves for a given transient experiment by varying U only. Figure 27 is a graph of calculated central-fuel and cladding-surface

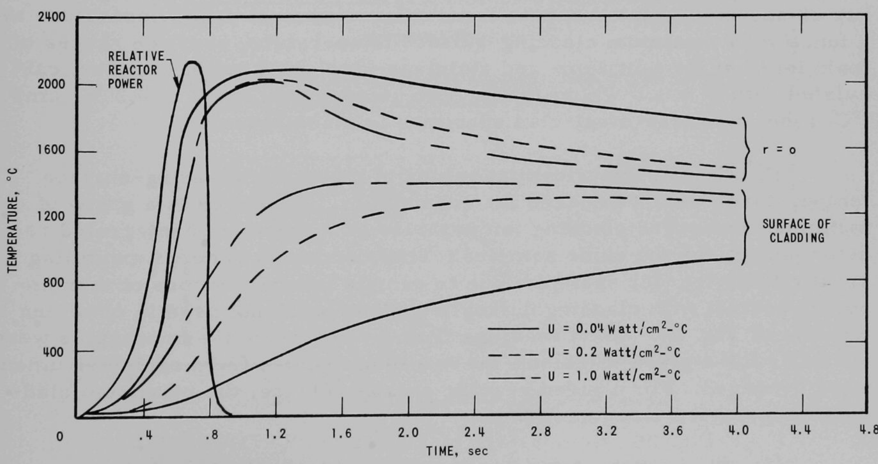

Fig. 27. Calculated Central-fuel and Cladding-surface Temperatures for Three Values of U

temperatures for three experimental arrangements identical except for U. For this example, maximum central-fuel temperature is insensitive to U, but the maximum cladding temperature and the time of maximum temperature are dependent upon U, at least over the range of 0.04-1 $W/(cm)^2(°C)$. A preliminary analysis of the value of U was made after the first series of experiments by comparing experimental and calculated cladding-surface temperatures. A value of 0.2 was obtained from a general comparison of cladding heating and cooling curve shapes. As a result of this study, a value of 0.2 was adopted for preliminary analysis of subsequent experiments. Estimated uncertainty in U as determined by this devious curve-matching method was set at a factor of 2.[31] It may be noted that a value of $U = 0.2\ W/(cm)^2(°C)$ is indicated for samples with these fuel-cladding clearances, for steady-state conditions.[15]

An attempt was made to obtain an effective U for the entire ensemble of experiments on the oxide specimens. Experimental values of the delay between maximum reactor power and maximum cladding temperature were compared with values calculated using experimental h, and U of 1.0, 0.2, and 0.04. The experimental numbers showed a wide scatter, but were concentrated between the theoretical curves defined by $U = 0.2$ and 1.0. No systematic deviations were noted for such experimental parameters as cladding material or maximum cladding temperature, but the general trend indicated a nominal value nearer 1.0 than 0.2.

From the above calculations, relationships were obtained between maximum central-fuel temperature and maximum cladding-surface temperature, and between maximum cladding-surface temperature and oxide sample temperatures at the time of maximum cladding temperature. Figure 28 shows calculated curves for maximum central-fuel temperature as a function of maximum cladding-surface temperature, over the ranges of main interest for tantalum- and stainless-steel-clad oxide samples, calculated with $U = 1.0\ W/(cm)^2(°C)$. For comparison, the $U = 0.2\ W/(cm)^2(°C)$ case, stainless-steel-clad specimen is also presented.

Finally, the experimental values of maximum cladding-surface temperatures were compared for consistency. Figure 29 is a graph of maximum measured cladding temperature as a function of integrated reactor power, for the oxide samples. Thermocouples records exhibiting erratic behavior (for example, due to sample failure, or loss of thermocouple contact with cladding during transient) were not used in obtaining the data of Fig. 29. When readings from two or more thermocouples were available for a given transient, the maximum values from each instrument were averaged. For a given reactor energy release, the maximum cladding temperature is a function of:

(1) Thermal-neutron flux depression due to both container and cladding material.

(2) The temperature distribution in the sample at the time of maximum cladding temperature.

(3) The sample heat lost to surroundings during the time of the cladding temperature rise.

(4) The heat content of the cladding.

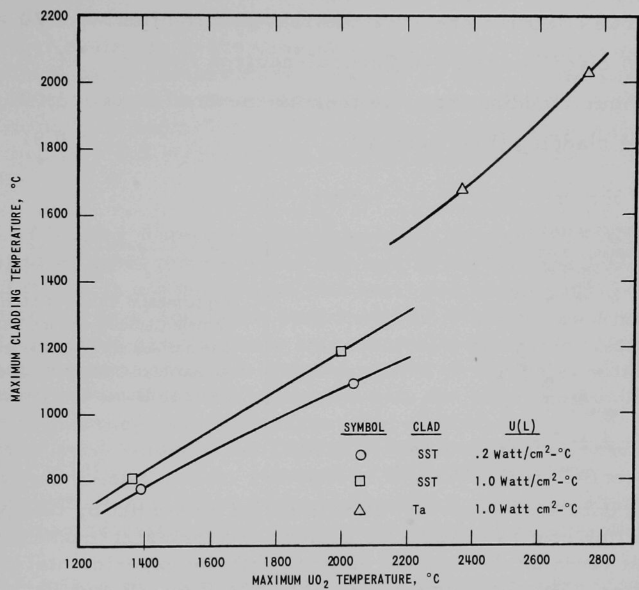

Fig. 28. Calculated Relationship between Maximum Oxide Sample Temperature and Maximum Cladding-surface Temperature

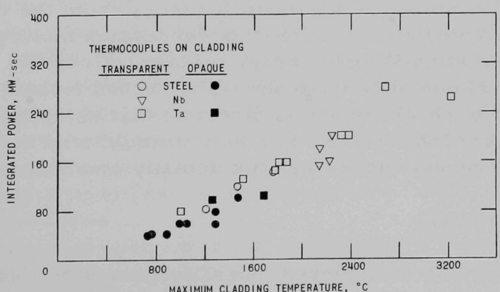

Fig. 29. Experimental Values of Maximum Sample Cladding-surface Temperature and Reactor Energy Release

Data of Fig. 29 were replotted in Fig. 30 by multiplying each value of integrated reactor power by a calculated coefficient equal to the ratio of reactor energy release for that sample to that for a tantalum-clad specimen that attained the same maximum cladding temperature as a result of exposure in the transparent meltdown facility. Correction factors used to normalize tantalum-clad samples in the transparent container were as follows:

Opaque container (relative thermal-neutron flux)	1.20
Steel cladding (relative thermal-neutron flux)	1.06
Niobium cladding (relative thermal-neutron flux)	1.07
Steel cladding (heat content)	0.91

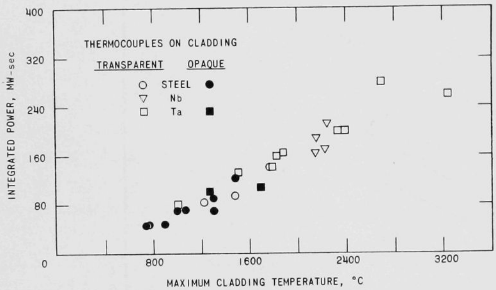

Fig. 30

Experimental Values of Maximum Sample Cladding-surface Temperature and Reactor Energy Release, Corrected to Uniform Sample and Thermal-neutron Flux Depression

The data scatter of Fig. 29 is reduced somewhat by this procedure for eliminating effects of variable nuclear and material properties. The scatter that remains thus should be typical of the experimental measurements proper. For the comparisons shown in Figs. 29 and 30, integrated reactor power is used instead of sample energy releases, because reactor power was measured directly in each experiment. Values of sample energy release for each experiment could have been estimated either from enthalpy values and experimental temperatures, or from the reactor integrated power values and calculated neutron-flux depression factors. The first technique for estimating sample energy release, of course, is not suitable for checking experimental consistency. The second technique, while suitable for this type of check, is not as direct as that using the reactor data and absolute calibration factors. Further, it would tend to obscure the fact that sample energy release was not actually measured.

B. Failure Calculations

For the samples considered, possible causes of cladding failure considered were:

(1) Cladding rupture due to differential thermal expansion.

(2) Cladding rupture due to internal pressure.

(3) Cladding rupture due to thermal stresses.

(4) Interaction between oxide and cladding.

These mechanisms may be reviewed briefly as follows:

1. Cladding Rupture due to Differential Thermal Expansion. No detailed calculations were made of cladding stresses due to thermal expansion of the fuel because of the presence of the gap between the fuel and the cladding. For example, in the case of a cladding tube held at room temperature, a uniform oxide temperature in excess of 1400°C would be required for the oxide to expand to the cladding inner surface. This type of temperature discontinuity is indicated by the transient temperature calculations, but even when $U = 0.2\ W/(cm)^2(°C)$, the discontinuity is not of sufficient magnitude.

2. Cladding Rupture due to Internal Pressure. Cladding rupture as a result of internal pressure buildup was estimated, using a simple, isothermal model in which the fuel, the inert gas bond, and the cladding were assumed to be at the same temperature. The internal volume was calculated. Internal gas pressure was computed using the perfect gas law, and cladding bursting pressure was calculated on the basis of a thin-walled cylinder.(31) Thermal expansion data for UO_2 over the temperature range of interest were taken from that of Halden et al.(32) Standard sources were used to obtain the thermal expansion coefficients for niobium and tantalum,*(33) and tensile strength of Type 304 stainless steel.(34) Tensile strength values for niobium and tantalum were obtained up to 2000°C,(35) and extrapolated to the melting points of the two metals.

Graphs showing calculated internal pressures and bursting pressures, plotted as functions of temperature, are shown as Figs. 31, 32, and 33 for steel-, niobium-, and tantalum-clad samples, respectively. In each case, internal pressure rises are modest and become equal to bursting pressure comparatively near the melting point of the cladding. For Type 304 stainless steel, this model predicts failure at 1377°C (4.8 atm); for niobium, at 1900°C (8.2 atm); and for tantalum, at 2393°C (12.2 atm). Because of the steep slope in the bursting-pressure curve of Fig. 31, comparatively large changes in the tensile-strength data would make only small changes in the temperature of intersection; however, even small changes in the bursting-pressure curves of Figs. 32 and 33 could effect appreciable changes in intersection temperature. This simple model does

*The average value over the range of 18-2000°C for niobium was $9.0 \times 10^{-6}/°C$. An average value of $8.1 \times 10^{-6}/°C$ was estimated for tantalum over the same range based on room-temperature values of 6.5×10^{-6} and 7.2×10^{-6} for niobium and tantalum, respectively.(31)

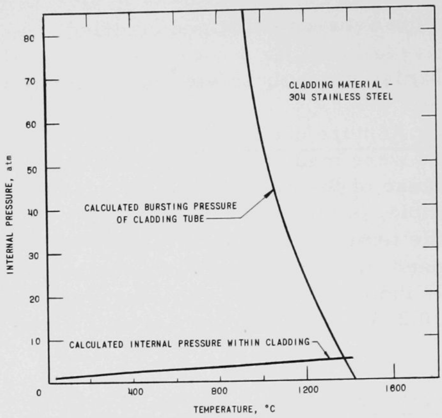

Fig. 31. Calculated Internal Pressure and Bursting Pressure for Isothermal 304 Stainless-steel-clad Sample

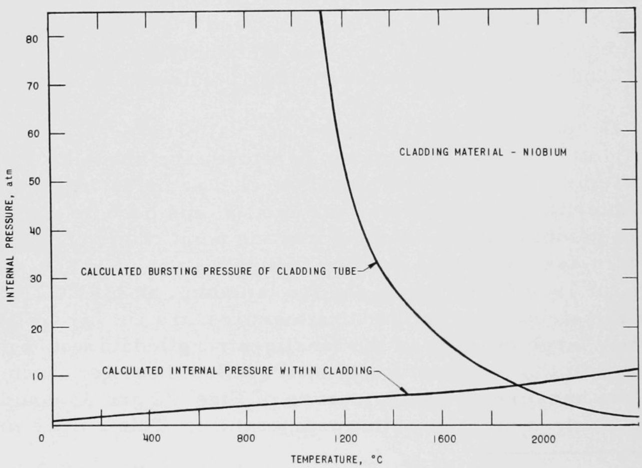

Fig. 32. Calculated Internal Pressure and Bursting Pressure for Isothermal Niobium-clad Sample

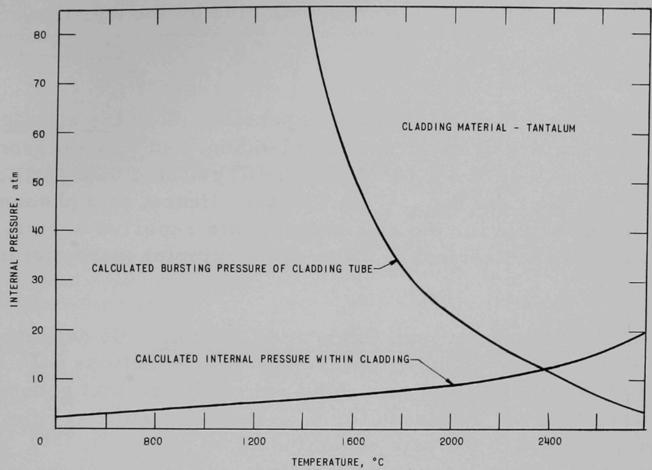

Fig. 33. Calculated Internal Pressure and Bursting Pressure for Isothermal Tantalum-clad Sample

not take into account possible defects in tube or end welds, nonuniform temperature distributions, or departure from elastic behavior at elevated temperatures. During the sample power input, oxide temperatures could be hundreds of degrees above that of the cladding, however. The isothermal approximation error due to this simplification is comparatively small. In the case of steel-clad specimens, the large negative first derivative of the bursting-pressure curve minimizes this effect; in the cases of niobium- and tantalum-clad samples, the absolute magnitudes of the first derivatives of the calculated bursting-pressure curves are less than those of the internal-pressure curves in the temperature ranges of interest. If one assumes that radial temperature distributions near peak cladding temperature may be approximated by a uniform oxide temperature 400°C above the cladding temperature, then failure occurs for Fig. 32 at about 1850°C (9.3 atm), and for Fig. 33 at 2290°C (14.7 atm). These differences are well within the large estimated uncertainties in the data used for calculations and uncertainties in temperature measurements.

3. Cladding Rupture due to Thermal Stresses. Thermal stresses in the cladding were estimated to be modest for these experiments. For purposes of orientation, transient temperatures were calculated for an oxide sample with the conservative value of $U = 0.2\ W/(cm)^2(°C)$, reaching a central temperature of about 2050°C above a slowly moving NaK-like coolant at 30°C surrounding the cladding. In that case, the maximum temperature drop in the cladding was 100°C. Maximum stress, σ_{max}, in the

thin shell of the cladding may be approximated by the equation[36]

$$\sigma_{max} = \alpha E(\Delta t)/[2(1 - \nu)], \qquad (2)$$

where α is the coefficient of thermal expansion, E is the elastic modulus, Δt is the temperature drop across the cladding, and ν is Poisson's ratio. Using values for steel of 2×10^{-5}°C, 24×10^{6} psi, and 0.28 for α, E, and ν, respectively, we have σ_{max} = 33,333 psi. Hence, this phenomenon would not be operative for the dry experiments reported herein, but would have to be considered seriously if the same samples were run in flowing sodium coolant.

4. Interaction between Oxide and Cladding. No definitive estimates were made of possible cladding failure due to interactions with oxide. Reaction of UO_2-stainless steel was ruled out on theoretical grounds.[37] No reaction was observed by Mason for UO_2-stainless steel cermet mixtures in differential thermal analysis experiments up to 1200°C.[38] Similarly, no reaction with either niobium or tantalum was indicated theoretically.*[37]

Experimentally, it has been reported that pellets of UO_2, placed in contact with niobium and tantalum, and run for 10 hr at 2000°C, were found to adhere to the metal. Examination of the metal-ceramic interfaces showed no "gross interaction but did indicate a penetration of the grain boundaries near the interface by some component from the UO_2."[39] Albaugh reported that molten UO_2 was found to react rapidly with tantalum, but the two materials were compatible below the UO_2 melting point.[40] Kerr,[18] however, found evidence for a "fast" reaction between UO_2 and tantalum at 2420°C. Another survey,[41] in which couples were exposed for 10 minutes at temperature in an argon atmosphere, reported niobium to be compatible with UO_2 up to the metal melting point, and tantalum to be compatible up to the oxide melting point.

C. Stress Estimates

Internal sample stresses arising from the calculated radial temperature distributions (see Section IV A, above) were calculated in order to estimate the likelihood of sample cracking, and the types of cracking that would occur. Standard equations were used for the plane-strain solutions for axial, radial, and tangential stresses in a right-circular cylinder due to a temperature distribution given as a function of radius.[42] These equations were coded for the IBM-704 computer by Miller,[43] and are valid for parts of the cylinder $\gtrsim$ one diameter from the ends. Figure 34 is a graph of calculated radial temperatures for selected times during a

---

*However, no directly measured values of free energy of formation were available in the temperature ranges of interest. Compatibility was estimated by extrapolating data from lower temperatures.

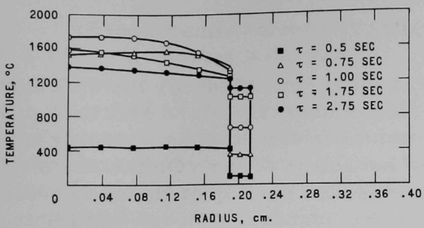

112-2875

Fig. 34. Calculated Radial Temperature Distribution for Typical Oxide Transient Experiment

typical energetic transient experiment. The general temperature profile is clearly concave upward at times near the time of maximum power (0.70 sec). Figure 35 shows the calculated radial, axial, and tangential stresses for two times near the power maximum (at 0.5 and 0.75 sec), and for three times during cooling (1.00, 1.75, and 2.75 sec). A value of 23 x 10^6 psi was used for the elastic modulus, α for the temperature range of interest was assumed to be 10^{-5}/°C, and ν was taken to be the room-temperature value of 0.3.(44) Stress values below zero in Fig. 35 represent compression; those above, tension. These calculations indicate that, for this case of modest thermal-neutron flux depression (see Table V), the stresses are not destructive up to a time (0.75 sec) past peak power, except at the edge of the oxide. There, the stresses are polar (produce radial cracking). Once cracking has occurred, direct application of this analysis to the cylinder is not justified because of the change in geometry. However, it may be noted a relatively well-defined central region of about 0.08-cm radius exists in which compressive stresses are excessive over 1.75 to 2.75 sec during the change from the initial temperature distributions when the cladding is heating up, to the distributions typical of cooling. These stress calculations should be interpreted as qualitative, both because they were performed for sintered ceramic bodies, which characteristically do not have uniform properties either from piece to piece or from point to point in a given piece, and because of the need to extrapolate material properties. A further qualification is Scott's report(45) that sintered UO_2 with an oxygen-to-uranium ratio of 2.06 and 2.16, and density above 95% of theoretical, can show plastic deformation at temperatures as low as 800°C. Stoichiometric uranium dioxide was found to deform plastically at temperatures above about 1600°C.(45)

Fig. 35

Calculated Radial, Axial, and Tangential Stresses for Two Calculated Temperature Distributions from Fig. 34

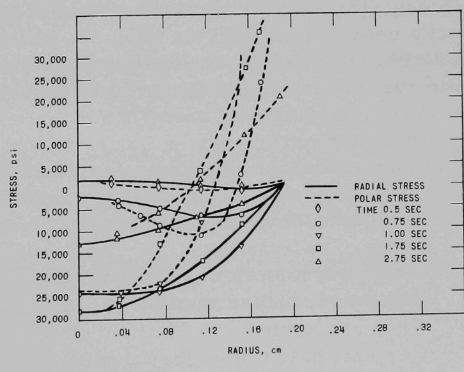

V. SUMMARY

Failure, in general, was comparatively nonviolent for the specimen types tested. For the stainless-steel-clad elements, failure occurred near the cladding melting point, close to the temperature at which cladding failure had been predicted with emission of hot internal gas. On the basis of a sample model, this was due to internal pressure buildup of the gas present inside the cladding when the element was fabricated. Although one failure was observed for a niobium-clad sample, that failure may not be at all typical since three other similar specimens were run to similar or higher temperature exposures. In the case of that one failure, the size of the cladding hole is about the size of molten drops in the center of the oxide cylinders (see Fig. 17), and a chance combination of distribution of the oxide cylinders within the cladding may have produced a melt-through. However, the edges of the hole were clearly defined, unlike the rounded edges that would be typical of melting. There were no bulges or bent-out edges around the hole, which implies that the failure was not due to internal pressure. The failure could also have been produced by some kind of brittle cracking,* but a possible mechanism for this has not been established. The three surviving high-temperature niobium-clad samples attained cladding temperatures about 200 to 300°C above that predicted to cause failure by pressure of the gas originally present inside the cladding. Partial explanations for this discrepancy may lie in the use of extrapolated data in the bursting calculations, and the appreciably increased cladding diameters noted in the post-experiment inspections of the niobium-clad samples.** The high-temperature failures of tantalum-clad elements, with the subsequent emission of molten fuel, appear to be in reasonable agreement with the failure prediction of the simple bursting model.

Onset of the appearance of the "recrystallized" central-oxide granular structure occurs for maximum central-fuel temperatures above the order of 2200°C (see Fig. 28). This central region may be associated with the high-stress central region found in the transient stress calculations (see Fig. 35). However, there is no accompanying appearance of radial cracks near or at the oxide surface, which also are predicted by the calculations. A possible explanation may be the relatively thin zone near the oxide surface, in which high polar stresses are calculated, combined with possible plastic deformation.[45]

---

*The appearance of fission products in the capsule cover gas system during the experiment proves that cladding failure occurred before the postexperiment handling.

**This increase in diameter would suggest that the niobium tubes merely expanded, rather than burst, from internal pressure.

Higher-temperature exposures tended to cause the oxide cylinders to break into shorter axial lengths. The cylinders did not exhibit the familiar pattern of radial and circumferential cracks typical of that displayed by fuel subjected to steady-state exposure. This, however, can be attributed to a difference in oxide thermal stresses between those arising from comparatively high-power, steady-state, radial-temperature distributions and those transient stresses arising in these experiments before the attainment of steady cooling of the sample.

"Glassy" central depressions in the ends of the oxide cylinders and/or well-formed drops of oxide appeared for estimated maximum central-fuel temperatures of approximately the uranium oxide melting point (see Fig. 28). Oxide cylinders from elements with estimated central-fuel temperatures of approximately the oxide melting point were found to have undergone small density increases.

It should be noted, however, that these tests do suggest that similar elements, in the presence of a typical "chopped-cosine" axial-power profile might exhibit a mode of failure analogous to a pattern found for sodium-bonded, metallic-fuel elements. In this case, failure might occur, preferentially in the region of highest power, and molten or badly cracked material along the axis would be forced axially to the region of failure.

These tests do not include possible effects produced by the presence of liquid-metal coolant, clustering of elements, or the variety of phenomena associated with appreciable prior irradiation. One sample, which was given a limited number of cycles of transient heating to a maximum cladding temperature about 300°C below the estimated failure threshold, maintained cladding integrity, but was found to have some fuel fragmentation.

ACKNOWLEDGMENTS

Assistance of the following ANL personnel is gratefully acknowledged:

The TREAT staff consisting of Manager J. F. Boland, Assistant Manager H. Lawroski, T. Kajor, G. P. Larson, F. S. Kirn, and R. D. DeForest.

J. H. Handwerk, F. D. McCuaig, and D. E. White of the Metallurgy Division.

J. H. Monaweck of the Reactor Engineering Division.

E. Simmons and C. August of the Reactor Physics Division.

REFERENCES

1. D. Okrent, "A Review of the Nuclear Aspects of Fast Reactor Safety," Physics of Fast and Intermediate Reactors, IAEA, Vienna, III, 155 (1962).
2. R. C. Liimatainen, R. O. Ivins, M. F. Deerwester, and F. J. Testa, Studies of Metal-Water Reactions at High Temperatures. II. TREAT Experiments: Status Report on Results with Aluminum, Stainless Steel-304, Uranium and Zircaloy-2, ANL-6250 (1962).
3. J. F. Boland, private communication (1961).
4. J. D. Eichenberg, P. W. Frank, T. S. Kisiel, B. Lustman, and K. H. Vogel, Effects of Irradiation of Bulk Uranium Dioxide, Fuel Element Conference, Paris, November 1957, TID-7546, Book 2 (1958), p. 616.
5. C. E. Dickerman, E. S. Sowa, and D. Okrent, Fast Reactor Safety Studies in TREAT - A Status Report, Nucleonics 19, No. 4, 114 (1961).
6. C. E. Dickerman, E. S. Sowa, D. Okrent, J. Monaweck, and L. B. Miller, Studies of Fast Reactor Fuel Element Behavior under Transient Heating to Failure. I. Initial Experiments on Metallic Samples in the Absence of Coolant, ANL-6334 (1961).
7. C. E. Dickerman, G. H. Golden, and L. E. Robinson, In-Pile Photographic Studies of EBR-II Mark I and Fermi 6re-A Sample Meltdown, Nucl. Sci. Eng. 14, No. 1, 30 (1962).
8. J. H. Field, F. J. Leitz, M. J. McNelly, and R. C. Nelson, Apparent Boiling of Uranium Oxide in the Center of a Fuel Pin during Transient Power Generation, Nucl. Sci. Eng. 14, No. 2, 210 (1962).
9. G. A. Freund, H. P. Iskenderian, and D. Okrent, "TREAT, A Pulsed Graphite-Moderated Reactor for Kinetics Experiments," Proc. Second Int. Conf., Geneva 10, 461 (1958).
10. G. A. Freund, P. Elias, D. R. MacFarlane, J. D. Geier, and J. F. Boland, Design Summary Report on the Transient Reactor Test Facility (TREAT), ANL-6034 (1960).
11. D. Okrent, C. E. Dickerman, J. Gasidlo, D. M. O'Shea, and D. F. Schoeberle, The Reactor Kinetics of the Transient Reactor Test Facility (TREAT), ANL-6174 (1960).
12. F. Kirn, J. F. Boland, R. D. Cook, and H. Lawroski, Reactor Physics Measurements in TREAT, ANL-6173 (1960).
13. C. E. Dickerman, R. D. Johnson, and J. Gasidlo, Kinetics of TREAT Used as a Test Reactor, ANL-6458 (1962).
14. G. H. Golden, C. E. Dickerman, and L. E. Robinson, Facility for Photographing In-pile Meltdown Experiments in TREAT, ANL-6457 (1962).

15. I. Cohen, B. Lustman, and J. D. Eichenberg, Measurement of the Thermal Conductivity of Metal-clad Uranium Oxide Rods during Irradiation, WAPD-228 (1960).

16. J. J. Byerley, The Compatibility of UO_2 with the Refractory Metals and Refractory Metal Thermocouples at Temperatures above 1750°C, CRFD-971 (1960).

17. I. E. Campbell, High Temperature Technology, John Wiley & Sons, Inc., New York (1956).

18. H. M. Kerr, Metallurgy Division Annual Progress Report for Period Ending September 1, 1959, p. 292, ORNL-2839 (1959).

19. J. E. Houghtaling, T. M. Quigley, and A. H. Spano, Calculation and Measurement of the Transient Temperature in a Low-enrichment UO_2 Fuel Rod during Large Power Excursions, IDO-16773 (1962).

20. D. E. White and J. H. Handwerk, Argonne National Laboratory, private communication.

21. E. J. Brooks, W. C. Kramer, and R. D. McGowan, High-temperature Sensors for BORAX-V Boiling Fuel Rods, ANL-6636 (1962).

22. J. Heestand, D. F. Schoeberle, and L. B. Miller, The Calculation of Transient Temperature Distributions in a Solid Cylindrical Pin, Cooled on the Surface, IBM-704 Program 524/RE-147, ANL-6237 (1960).

23. J. Heestand, D. F. Schoeberle, and L. B. Miller, A Method of Calculating Transient Temperatures in a Multiregion, Axisymmetric, Cylindrical Configuration, The ARGUS Program, 1089/RE-248, Written in FORTRAN II, ANL-6654, (1963).

24. R. D. Reiswig, Thermal Conductivity of UO_2 to 2100°C, J. Am. Ceram. Soc. 44, 48 (1961).

25. R. Scott, Thermal Conductivity of Uranium Dioxide, AERE M/R 2526 (1958).

26. J. L. Bates, Thermal Conductivity of UO_2 Improves at High Temperatures, Nucleonics 19, No. 6, p. 83 (1961).

27. T. E. Tietz and J. W. Wilson, Mechanical, Oxidation, and Thermal Property Data for Seven Refractory Metals and Their Alloys, ASTIA AD-266824; NP-11108 (1961).

28. R. E. Taylor and R. A. Finch, The Specific Heats and Resistivities of Molybdenum, Tantalum, and Rhenium from Low to Very High Temperatures, NAA-SR-6034 (1961).

29. Quarterly Report, July, August, and September 1957, Metallurgy Division, ANL-5797 (1957).

30. J. Belle, ed., Uranium Dioxide - Properties and Nuclear Applications, U. S. Govt. Printing Office, Washington, D. C., 1961, Table 5.6.

31. W. Goodwin, unpublished Argonne National Laboratory memorandum (1961).

32. F. A. Halden, H. C. Wohlers, and R. H. Reinhart, Thermal Expansion of Uranium Dioxide, Stanford Research Institute, TID-5722 (1959).

33. C. R. Tipton, Jr. (ed.), Reactor Handbook (Second Edition) Vol. 1, Materials (New York: Interscience Publishers, Inc. 1960).

34. T. Lyman (ed.), Metals Handbook (The American Society for Metals, 1948).

35. B. L. Mordike, The Tensile Strength of Some Refractory Metals at High Temperatures, J. Inst. Metals 88, 272 (1960).

36. S. Timoshenko, Strength of Materials, Part II, Second Edition (New York: D. Van Nostrand 1943).

37. A. Glassner, The Thermochemical Properties of the Oxides, Fluorides, and Chlorides to 2500°K, ANL-5750 (1957).

38. Chemical Engineering Division Summary Report, January, February, March 1961, ANL-6333 (1961).

39. A. Weinberg and L. Yang, Interdiffusion between Uranium-bearing Reactor Fuels and Refractory-metal Thermionic Emitter, GA-3124 (1962).

40. F. W. Albaugh, Cited in Reactor Core Materials 4, No. 4 (1961), p. 11.

41. J. J. Gangler, W. A. Sanders, and I. L. Drell, Uranium Dioxide Compatibility with Refractory Metals, Carbides, Borides, Nitrides, and Oxides between 3500° and 5000°F, NASA Tech. Note D-262.

42. B. A. Boley and J. H. Weiner, Theory of Thermal Stresses (New York: John Wiley & Sons Company, 1960).

43. L. B. Miller, Argonne National Laboratory, private communication.

44. S. M. Lang, Properties of High Temperature Ceramics and Cermets, Elasticity and Density at Room Temperature, Nat. Bur. Stand. Monograph 6, March 1960.

45. R. Scott, A. R. Hall, and J. Williams, The Plastic Deformation of Uranium Oxides above 800°C, J. Nucl. Mat. 1, 39 (1959).

X